This article has been accepted for publication in a future issue of this journal, but has not been fully edited. Content may change prior to final publication. Citation information: DOI 10.1109/TCSII.2018.2875591, IEEE Transactions on Circuits and Systems II: Express Briefs

Complementarity Model for Steady-State Analysis of Resonant LLC Power Converters

Valentina Sessa ♮*Member, IEEE*, Luigi Rubino◇, Luigi Iannelli♮ *Senior Member, IEEE*, Francesco Vasca♮ *Senior Member, IEEE*, Pompeo Marino◇

***Abstract*—In recent years, the complementarity formalism has been shown to be an interesting framework for the mathematical representation of a large class of power converters. In this paper, the complementarity model of a resonant LLC power converter is presented. The model usefulness is demonstrated for the identification of the circuit parameters and for the numerical analysis of the stationary behavior. The comparison between experimental measurements and numerical results shows the efficacy of the proposed approach.**

***Index Terms*—Power converters; resonant circuits; steady-state behavior; complementarity models.**

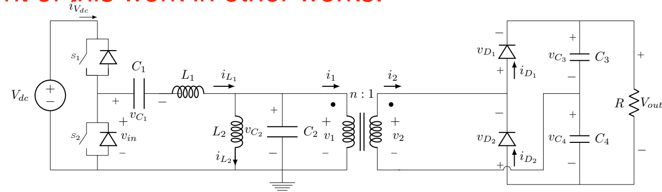

Figure 1. An equivalent circuit of the resonant LLC power converter considered in this paper.

I. Introduction

The resonant LLC converter is an emerging topology to meet the high efficiency and power density requirements necessary in industrial applications, see among the others [1]–[3]. The computation and analysis of the steady-state behavior in power converters is a critical issue [4]–[6] since it requires to know the operating modes sequence and the switching time instants. For resonant converters, the steady-state analysis is often carried out by an extensive enumeration and description of all the operating conditions [4], [7], [8]. The electronic switches states lead to different circuit topologies, i.e. the so-called *modes*. The concatenation procedure of the corresponding dynamic models is quite costly as the number of switches can be high. Moreover, the resulting model is usually in a non explicit form due to the switching conditions, which represent time- and state-dependent algebraic constraints.

In the seminal work [9], linear complementarity models have been used to build a compact representation of power converters. Such class of models is simple to be built and does not require the a priori knowledge of the converter modes nor the switching time instants. In fact, a unique mathematical model describes the power converter behavior in all operating conditions. Complementarity models have shown to be effective in capturing the dynamic behavior of power converters [10]–[13]. Moreover, the steady-state solution of the discretized complementarity model can be directly computed without fixing the sequence of modes, which is not known, for instance, when diodes influence the circuit behavior, such as in discontinuous conduction mode [11], [12]. Specific conventional open-loop power converters topologies such as single-phase diode bridges [14], three-phase rectifiers [15], and resonant converters [11] have been modeled and analyzed within the complementarity framework. Recently, those models have been extended also to closed-loop power converts such as Čuk converter [16], Z-converter [12], buck-boost converter [17] and single-phase multilevel converters [18]. In the literature, the numerical solution of complementarity models is usually compared with the solution of other solvers without proposing experimental validations. In this paper, by considering a dedicated resonant LLC converter prototype, several comparisons with experimental results show the effectiveness of the complementarity model. It is worthy to mention that the proposed procedure can be applied to derive complementarity models of more complex circuit topologies too, e.g. by considering linear sub-circuits which model the effects of parasitic elements and piecewise linear characteristics of electronic devices [9]. We decided to maintain a compromise between the complexity of the model, without introducing many circuit details, and the fidelity in reproducing the experimental results in a sufficiently wide range of different operating conditions. As a further original contribution, the use of these models for parameters identification based on the steady-state response is proposed.

The paper is organized as follows. In Section II, the dynamic model of the LLC converter and the complementarity problem providing its steady-state solution are presented. The experimental prototype is described in Section III and the parameters identification in Section IV. The effectiveness of our approach for the steady-state analysis is discussed in Section V. The conclusions are reported in Section VI.

II. Complementarity model of LLC converter

In this section, we derive the dynamic complementarity model of the resonant LLC converter shown in Fig. 1. The discretized model is then combined with periodicity conditions thus obtaining a *mixed linear complementarity problem*

(♮) Dipartimento di Ingegneria, Università del Sannio, Piazza Roma 21, 82100 Benevento, Italy, email: sessa.valentina@gmail.com, {francesco.vasca, luigi.iannelli}@unisannio.it

(◇) Dipartimento di Ingegneria, Università della Campania Luigi Vanvitelli, Via Roma 29, 81031 Aversa (Caserta), Italy, email: {luigi.rubino, pompeo.marino}@unicampania.it

(MLCP) whose solution provides the steady-state evolution of the power converter electrical variables.

A. Dynamic model

Let us consider the resonant LLC power converter in Fig. 1. The two switches S_1 and S_2 are controlled in anti–phase with a switching frequency f_s. The modulation determines a square wave voltage v_{in} with amplitude V_{dc}. The capacitor C_1 and the inductors L_1 and L_2 constitute a resonant circuit. A transformer is used to connect the resonant circuit to a diode rectifier, which is usually operated in discontinuous conduction mode. The ideal transformer relations $v_1 = nv_2$ and $i_2 = ni_1$ are used. By applying the Kirchhoff laws, one obtains

$$
\begin{aligned}
L_1 \mathcal{D} i_{L_1} &= -v_{C_1} - v_{C_2} + v_{in} && \text{(1a)}\\
C_1 \mathcal{D} v_{C_1} &= i_{L_1} && \text{(1b)}\\
L_2 \mathcal{D} i_{L_2} &= v_{C_2} && \text{(1c)}\\
C_2 \mathcal{D} v_{C_2} &= i_{L_1} - i_{L_2} - {}^1\!/_n i_{D_1} + {}^1\!/_n i_{D_2} && \text{(1d)}\\
C_3 \mathcal{D} v_{C_3} &= i_{D_1} - {}^1\!/_R v_{C_3} - {}^1\!/_R v_{C_4} && \text{(1e)}\\
C_4 \mathcal{D} v_{C_4} &= i_{D_2} - {}^1\!/_R v_{C_3} - {}^1\!/_R v_{C_4} && \text{(1f)}\\
v_{D_1} &= {}^1\!/_n v_{C_2} - v_{C_3} && \text{(1g)}\\
v_{D_2} &= -{}^1\!/_n v_{C_2} - v_{C_4}, && \text{(1h)}
\end{aligned}
$$

where $\mathcal{D}x$ stands for the time derivative of x. Let us introduce the vectors $z^\top = (i_{D_1}\, i_{D_2})$ and $w^\top = (-v_{D_1}\, -v_{D_2})$, the input $u = v_{in}$ and the state vector $x^\top = (i_{L_1}\, v_{C_1}\, i_{L_2}\, v_{C_2}\, v_{C_3}\, v_{C_4})$. Then, (1) can be rewritten in the matrix form

$$
\begin{aligned}
\mathcal{D}x &= A_c x + B_c z + E_c u && \text{(2a)}\\
w &= C_c x + D_c z + F_c u, && \text{(2b)}
\end{aligned}
$$

where $x \in \mathbb{R}^6$, $u \in \mathbb{R}$, $z \in \mathbb{R}^2$ and $w \in \mathbb{R}^2$, and A_c, B_c, C_c, D_c, E_c, F_c are real matrices of suitable dimensions. The complementarity model of the circuit is obtained by combining (2) with the complementarity representation of the diodes characteristics. An ideal diode model corresponds to a conducting mode when its current i_D is positive with zero voltage, whereas it is blocking when the opposite of its voltage, i.e. $-v_D$, is positive with zero current. Then, each ideal diode characteristic can be completely represented by the so-called complementarity condition $0 \le (-v_D) \perp i_D \ge 0$, where $-v_D$ and i_D are called complementary variables and the symbol $\perp$ represents the orthogonality constraint $-v_D i_D = 0$. By considering the two pairs of diodes variables in (1), the complementarity conditions of these two electronic devices can be written in the vector form

$$
0 \le w \perp z \ge 0, \tag{3}
$$

where the orthogonality is meant componentwise, i.e. $w_i = -v_{D_i} \ge 0$, $z_i = i_{D_i} \ge 0$ and $w_i z_i = 0$ for $i = 1, 2$. The set of expressions (2)–(3) is a continuous-time linear complementarity system. It represents in a compact form any mode of the power converter, i.e. it holds independently of the conducting or blocking states of the diodes and for continuous and discontinuous conduction modes too [12]. Moreover, this model allows one to directly compute the steady-state solution without assuming the knowledge of modes sequence. This is shown in the following section.

B. Steady-state solution

In ordinary operating conditions, the input v_{in} of the resonant power converter is periodic of period $T_s = 1/f_s$ and the state variables show a periodic behavior with a period that is a multiple of the external forcing: in other words, we have subharmonics in the state [19]. Thus, in order to obtain the control-to-output frequency response, the input v_{in} is assumed to be periodic with period αT_s, α being a suitable integer.

The first step for the numerical computation of the resonant converter steady-state response consists of discretizing (2)–(3). Let us consider a sampling period, say h. Without loss of generality one can assume $h = \alpha T_s / N$, where N is a positive integer. The continuous-time state derivative at the time instant kh with $k = 1, 2, ...$ can be approximated as $\mathcal{D}x \simeq (x_k - x_{k-1})/h$, where x_k is the k-th sample of the discretized model vector state. Then, by using the backward Euler discretization technique with sampling period h, from (2)–(3) one obtains the following discrete-time system

$$
\begin{aligned}
0 &= -A x_k + B z_k + E u_k + x_{k-1} && \text{(4a)}\\
w_k &= C_c x_k + D_c z_k + F_c u_k && \text{(4b)}\\
0 &\le w_k \perp z_k \ge 0, && \text{(4c)}
\end{aligned}
$$

with $A = I - hA_c$, $B = hB_c$, $E = hE_c$, and k being positive. At each time-step k, given x_{k-1} and u_k, the set of expressions (4) is an MLCP in terms of unknown (x_k, z_k) whose solution can be obtained by using the well-known PATH solver [12]. Then, starting from a given x_0 and the knowledge of the input u_k for $k = 1, 2, ...$, the whole state evolution can be obtained by iteratively solving for $k = 1, 2, ...$ the sequence of MLCPs (4).

Since v_{in} is periodic of period αT_s, from the definition of h given above, the sampled discrete-time input u_k is periodic of period N. A big MLCP for the computation of the steady-state solution can be obtained by collecting in a vector form the expressions (4) for $k = 1, 2, ..., N$ and by replacing x_0 with x_N in (4a) for $k = 1$, thus exploiting the periodicity assumption $x_0 = x_N$. Let us define $\bar{x} = \mathrm{vec}(\{x_i\}_{i=1}^N) \in \mathbb{R}^{6N}$, $\bar{u} = \mathrm{vec}(\{u_i\}_{i=1}^N) \in \mathbb{R}^N$, $\bar{z} = \mathrm{vec}(\{z_i\}_{i=1}^N) \in \mathbb{R}^{2N}$, and $\bar{w} = \mathrm{vec}(\{w_i\}_{i=1}^N) \in \mathbb{R}^{2N}$, where vec indicates the vectorization operator. Then, the set of (4) for $k = 1, ..., N$ with $x_0 \leftarrow x_N$ can be written as the following big MLCP:

$$
\begin{aligned}
0 &= \overline{A}\overline{x} + \overline{B}\overline{z} + \overline{E}\,\overline{e} && \text{(5a)}\\
\overline{w} &= \overline{C}\overline{x} + \overline{D}\overline{z} + \overline{F}\,\overline{e} && \text{(5b)}\\
0 &\le \overline{w} \perp \overline{z} \ge 0, && \text{(5c)}
\end{aligned}
$$

where the block circulant matrix $\bar{A}$ is defined as

$$
\bar{A} = \begin{pmatrix}
-A & 0 & \cdots & \cdots & 0 & I \\
I & -A & 0 & \cdots & \cdots & 0 \\
0 & I & -A & 0 & \cdots & \vdots \\
\vdots & \ddots & \ddots & \ddots & \ddots & \\
0 & \cdots & 0 & I & -A & 0 \\
0 & 0 & \cdots & 0 & I & -A
\end{pmatrix},
$$

$\overline{B} = I_N \otimes B_c$, $\overline{E} = I_N \otimes E_c$, $\overline{C} = I_N \otimes C_c$, $\overline{D} = I_N \otimes D_c$, $\overline{F} = I_N \otimes F_c$, with I_N being the N-dimensional identity matrix and the symbol $\otimes$ indicating the Kronecker product.

This article has been accepted for publication in a future issue of this journal, but has not been fully edited. Content may change prior to final publication. Citation information: DOI 10.1109/TCSII.2018.2875591, IEEE Transactions on Circuits and Systems II: Express Briefs

The solution $(\overline{x}, \overline{z})$ of the MLCP (5) provides directly the evolution of the converter state variables at steady-state. Note that alternative discretization schemes could be used without affecting the validity of the proposed procedure, just requiring to modify accordingly the matrices in (5). In most cases, the backward Euler discretization technique is preferred for complementarity systems due to its stability property [14].

III. Experimental prototype

An experimental prototype shown in Fig. 2 has been built to validate the linear complementarity model. The converter is sized for $5\,\mathrm{kW}$ and the nominal operating characteristics, referred to the converter working at the resonance frequency are: input voltage $84\,\mathrm{V}$, input current $60\,\mathrm{A}$, output voltage $28\,\mathrm{V}$, and output current $180\,\mathrm{A}$. The resonance frequency has been fixed at $110\,\mathrm{kHz}$ and the converter can work up to $300\,\mathrm{kHz}$ in order to regulate the output voltage in wide ranges of the input voltage and load. The nominal circuit parameters are: $L_1 = 1.24\,\mu\mathrm{H}$, $C_1 = 2.2\,\mu\mathrm{F}$, $C_3 = 35.2\,\mu\mathrm{F}$, and $C_4 = 35.2\,\mu\mathrm{F}$. The parameters L_2 and C_2 will be identified in next section.

The inductance L_1 represents the sum of the transformer leakage inductance and the external resonance inductance of Fig. 2(c). The transformer in Fig. 2(d) is custom made and the main parameters considered for the transformer design are the reduction of losses, weight and volume. A strong interleaved method in the coil arrangement was used following the procedure described in [2]. The final transformer design provided the following parameters: transformer turn ratio $n = 3$; core material 3C94; core shape E43/10/28; insulator is polymide; insulation thickness $0.025\,\mathrm{mm}$; copper thickness primary $0.45\,\mathrm{mm}$; copper thickness secondary $1.35\,\mathrm{mm}$; interleaving scheme is 0.5P, S, P, S, P, S, 0.5P.

One of the most critical components of the LLC converter is the resonant capacitor C_1 placed in series to the circuit and working with the nominal current. The current is responsible of the temperature increasing due to the Joule effect. The high temperature may destroy the capacitor if it reaches the dielectric limits. For this reason, low series resistance capacitor is required for the application. Another limit is given by the voltage that must be always under the dielectric limits. Furthermore, the capacitance value may change with the temperature, making the converter parameters temperature dependent. All the above mentioned limits have been solved by selecting the NPO (COG) ceramic capacitor that can work up to $10\,\mathrm{MHz}$ with small losses, small temperature dependence, high working voltage and with no aging. A custom capacitor construction has been adopted to select the best devices on the market. The capacitor prototype is shown in Fig. 2(b) and is obtained by paralleling 100 small capacitors, each working with a fraction of the total current.

The driver dsPIC33FJ16GS504 was used to generate the PWM signal at the desired frequency. The DSP configurations, e.g. PWM frequency, duty cycle and dead time, can be changed during the tests via the RS232 serial communication. For measurements accuracy a wide band oscilloscope and current sensor (CWT06B $50\,\mathrm{mV/A}$ $120\,\mathrm{A}$ POWERTEK) was used.

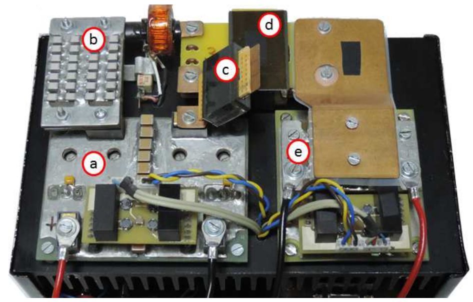

Figure 2. Experimental 5 kW prototype. (a) Half bridge (b) resonant capacitor (c) resonant inductor (d) transformer (e) rectifier. Size: 17x10 cm.

IV. Parameters identification

In this section, we show how the parameters L_2 and C_2 have been identified by exploiting the proposed model. The elements L_2 and C_2 cannot be considered properly as lumped circuit representations of physical elements, because they also synthesize complex unmodeled parasitic elements. In particular, the parasitic phenomena related to the transformer magnetization inductance L_2 are due to the busbar capacitance, the proximity and skin effect losses. The capacitor C_2 includes effects of winding and diode capacitance. These phenomena could be modeled by using complex equivalent circuits. However, by neglecting the parasitic elements, one can reduce the circuit complexity to the one considered in Fig. 1, with frequency-dependent parameters.

Measurements of the input voltage, the current through the inductor L_1, and the voltage across the two input inductors have been performed at steady-state conditions with different switching frequencies. The data acquisition was performed with a sampling period equal to $0.2\,\mathrm{ns}$. The measured signal v_{in} (resampled at $20\,\mathrm{ns}$) was used as input for the MLCP (5). Then the physical circuit and the mathematical model have the same input waveform.

We considered twenty values for L_2 and C_2 in the intervals $[3, 50]\mu\mathrm{H}$ and $[1, 40]\mathrm{nF}$, respectively. For each pair (L_2, C_2), we computed the steady-state solution by solving the corresponding MLCP (5) at each switching frequency. We computed the root mean square error (RMSE) for the current through the inductor L_1 as follows:

$$\mathrm{RMSE} = \sqrt{\frac{1}{N}\sum_{k=1}^{N} \|\hat{i}^k_{L_1} - \overline{i}^k_{L_1}(L_2, C_2)\|^2}, \tag{6}$$

where $\hat{i}^k_{L_1}$ is the k-th sample (with respect to a chosen initial phase) of the measured current, $\overline{i}^k_{L_1}(L_2, C_2)$ is the k-th sample of the computed inductor current, and N is the period of the discrete-time input signal. In Fig. 3, we show the RMSE map at the switching frequency $f_s = 100\,\mathrm{kHz}$. The red star represents the optimal point corresponding to the computed optimal values (L_2^*, C_2^*).

In Table I, for each pair of parameters values (L_2^*, C_2^*), which are optimal for a selected frequency, we computed the RMSE for i_{L_1}, when this pair of parameters is considered for computing the steady-state solution at different frequencies.

This article has been accepted for publication in a future issue of this journal, but has not been fully edited. Content may change prior to final publication. Citation information: DOI 10.1109/TCSII.2018.2875591, IEEE Transactions on Circuits and Systems II: Express Briefs

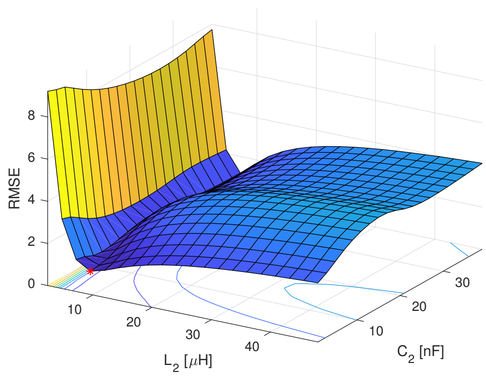

Figure 3. Root mean square error map for the current i_{L_1} by varying L_2 and C_2 at $f_s = 100\,\mathrm{kHz}$.

Table I
RMSE FOR THE CURRENT THROUGH THE INDUCTOR L_1.

(L_2^*, C_2^*) at f	RMSE for i_{L_1}			
	80 kHz	100 kHz	200 kHz	300 kHz
(36 μH, 1 nF)@80 kHz	0.670	4.58	2.22	3.40
(9.6 μH, 1 nF)@100 kHz	2.60	1.10	4.26	3.73
(48 μH, 17 nF)@200 kHz	1.66	2.30	0.236	0.842
(38.4 μH, 31 nF)@300 kHz	1.82	2.09	0.680	0.243

On the main diagonal of the above table, we highlighted the optimal value corresponding to each of the four frequencies.

V. STEADY-STATE BEHAVIOR

In this section, we provide a validation of the complementarity model for the computation of the converter steady-state solution by comparing numerical and experimental results for different switching frequencies and load resistances.

Figure 4 shows the comparison between the experimental measurements (continuous blue line), MLCP (dashed red line) and PLECS steady-state solutions (dash-dotted green line) at $f_s = 80\,\mathrm{kHz}$ and $f_s = 100\,\mathrm{kHz}$. The RMSE for the current i_{L_1} computed between the measured current and PLECS results when $f_s = 100\,\mathrm{kHz}$ is 5.39, whereas it is 1.10 when MLCP solution is considered, so as shown in Table I. MLCP results are very close to the measurements. That is a first validation of the effectiveness of the complementarity approach, which accurately captures the converter steady-state behavior. The cpu time for computing the steady-state solution at $f_s = 80\,\mathrm{kHz}$ with $h = 0.025\,\mu\mathrm{s}$ is around $0.35\,\mathrm{s}$ on an Intel Core i7 $2.40\,\mathrm{GHz}$. This value is comparable to that required by PLECS/Steady-State Analysis Tool, which is around $0.33\,\mathrm{s}$. It is important to mention here that MLCP steady-state solution is computed by applying the exact periodicity constraint, whereas in PLECS a relative error of 10^{-8} is selected.

Let us consider the input current $i_{V_{dc}}$ by assuming (it is an ideal behavior) that it coincides with i_{L_1} when the switch S_1 is conducting and it is zero when S_2 is turned on. The spectra of the currents i_{L_1} and $i_{V_{dc}}$ in Fig.s 5(a) and 5(b) show that the complementarity model efficiently reproduces the experimental converter behavior.

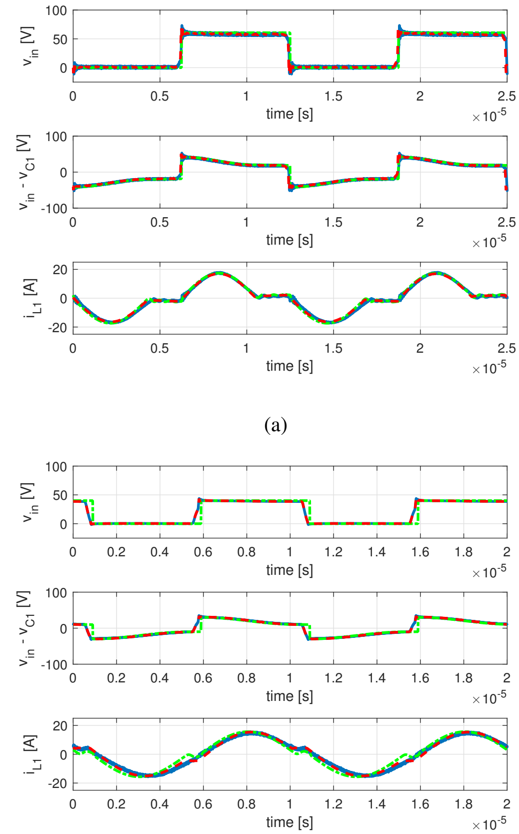

(a)

(b)

Figure 4. Comparison between the experimental results (continuous blue line), MLCP steady-state solution (dashed red line) and PLECS steady-state solution (dash-dotted green line) : (a) $V_{dc} = 60.6\,\mathrm{V}$, $R = 1.7\,\Omega$, $f_s = 80\,\mathrm{kHz}$. (b) $V_{dc} = 40\,\mathrm{V}$, $R = 1\,\Omega$, $f_s = 100\,\mathrm{kHz}$.

A further validation is made through the converter input-output characteristic. Define the voltage ratio as V_{out}/V_{dc}, where V_{out} is the average value over the period T_s of the output voltage at steady-state. Experimental measurements of the voltage ratio for different values of the switching frequency in the interval between $80\,\mathrm{kHz}$ and $300\,\mathrm{kHz}$ were performed. In Fig. 6, we report the comparison of the experimental values with MLCP and PLECS steady-state solutions for two different values of the output resistor. Instead of using the different pairs (L_2^*, C_2^*), we fixed these parameters to the mean of their optimal values at the different frequencies. In this case in the MLCP models, a constant voltage drop has been used for each diode. MLCP results fit quite well the measurements. It should be noticed that PLECS steady-state tool requires small series resistors at the transformer output and in series with L_1 and C_2 in order to get the convergence, whereas this is not necessary for computing MLCP solutions.

VI. CONCLUSION

The complementarity theory has been applied for modeling a resonant LLC power converter. This mathematical representation catches the converter behavior in all operating modes and allows one to directly compute the steady-state converter

This article has been accepted for publication in a future issue of this journal, but has not been fully edited. Content may change prior to final publication. Citation information: DOI 10.1109/TCSII.2018.2875591, IEEE Transactions on Circuits and Systems II: Express Briefs

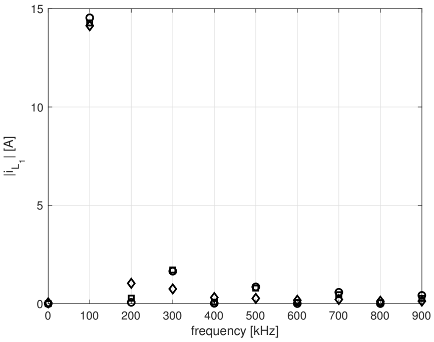

(a)

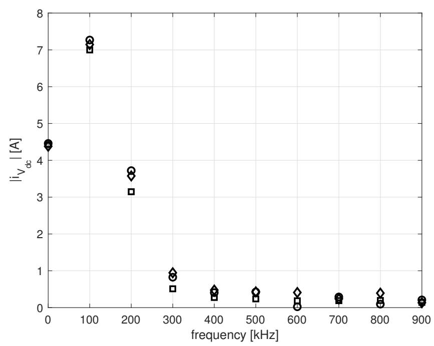

(b)

Figure 5. Spectra: (a) current through the inductor, i_{L_1} and (b) input current, $i_{V_{dc}}$: experimental measurements (diamonds), MLCP steady-state solution (squares) and PLECS solution (circles) for $V_{dc} = 40\,\mathrm{V}$ at $f_s = 100\,\mathrm{kHz}$ with $(L_2, C_2) = (L_2^*, C_2^*)$ and $R = 1\,\Omega$

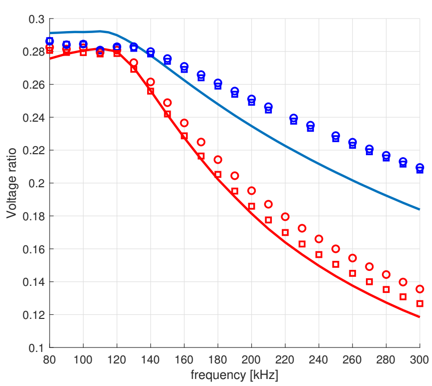

Figure 6. Comparison between the experimental measurements (continuous line), MLCP steady-state solution (squares) and PLECS solution (circles): voltage ratio V_{out}/V_{dc} vs. switching frequency f_s with $L_2 = 33\,\mu\mathrm{H}$, $C_2 = 12.5\,\mathrm{nF}$, $R = 0.54\,\Omega$ (red) and $R = 1.04\,\Omega$ (blue).

solution in a short computational time and by considering the exact periodicity constraint. An experimental prototype was built to validate the model and a comparison with experimental results have shown that the complementarity model accurately predicts the converter behavior. Mixed linear complementarity problems have been shown to be a powerful tool for the frequency dependence analysis of the circuit parameters and of the power converter input-output behavior. Linear complementarity systems provide a compact representation which could be further exploited for the converter design. Directions of future research are the use of these models for the analysis of system's properties, e.g. stability, controllability, observability, for the control design of power converters and for their analysis in the presence of nonlinear components.

REFERENCES

[1] T. Qian, "A converter combination scheme for efficiency improvement of PV systems," *IEEE Trans. Circuits Syst. II, Exp. Briefs*, vol. to appear, 2017.

[2] G. Rubino, L. Rubino, N. Serbia, P. Ladoux, and P. Marino, "LLC resonant converters in PV applications comparison of topologies considering the transformer design," in *IEEE Int. Conf. on Clean Electrical Power*, Alghero, Italy, June 2013, pp. 37–41.

[3] T. S. Chan and C. L. Chen, "A primary side control method for wireless energy transmission system," *IEEE Trans. Circuits Syst. I, Reg. Papers*, vol. 59, no. 8, pp. 1805–1814, 2012.

[4] A. E. Aroudi, M. S. Al-Numay, W. G. Lu, J. M. Bosque-Moncusí, and H. H. C. Iu, "A combined analytical-numerical methodology for predicting subharmonic oscillation in H-bridge inverters under double edge modulation," *IEEE Trans. Circuits Syst. I, Reg. Papers*, vol. to appear, 2017.

[5] H.-P. Park and J.-H. Jung, "PWM and PFM hybrid control method for LLC resonant converters in high switching frequency operation," *IEEE Trans. Ind. Electron.*, vol. 64, no. 6, pp. 253–263, 2017.

[6] R. Trinchero, P. Manfredi, I. S. Stievano, and F. Canvero, "Steady-state analysis of switching converters via frequency-domain circuit equivalents," *IEEE Trans. Circuits Syst. II, Exp. Briefs*, vol. 63, no. 8, pp. 748–752, 2016.

[7] R. Yang, H. Ding, Y. Xu, L. Yao, and Y. Xiang, "An analytical steady-state model of LCC type series-parallel resonant converter with capacitive output filter," *IEEE Trans. Power Electron.*, vol. 29, no. 1, pp. 328–338, 2014.

[8] C. Liu, H. Liu, G. Cai, S. Cui, H. Liu, and H. Yao, "Novel hybrid LLC resonant and DAB linear DC–DC converter: Average model and experimental verification," *IEEE Trans. Ind. Electron.*, vol. 64, no. 9, 2017.

[9] F. Vasca, L. Iannelli, M. K. Camlibel, and R. Frasca, "A new perspective for modeling power electronics converters: Complementarity framework," *IEEE Trans. Power Electron.*, vol. 24, no. 2, pp. 456–468, 2009.

[10] J. Tant, J. Driesen, and W. Michiels, "Event-driven simulation of power electronics in the complementarity systems framework," in *13th IEEE Workshop on Control and Modeling for Power Electronics*, Kyoto, Japan, June 2012, pp. 1–7.

[11] L. Iannelli, F. Vasca, and G. Angelone, "Computation of steady–state oscillations in power converters through complementarity," *IEEE Trans. Circuits Syst. I, Reg. Papers*, vol. 58, no. 6, pp. 1421–1432, 2011.

[12] V. Sessa, L. Iannelli, and F. Vasca, "A complementarity model for closed-loop power converters," *IEEE Trans. Power Electron.*, vol. 29, no. 12, pp. 6821–6835, 2014.

[13] K. Addi and D. Goeleven, *Complementarity and Variational Inequalities in Electronics*. Springer International Publishing, 2017, pp. 1–43.

[14] V. Acary, O. Bonnefon, and B. Brogliato, *Nonsmooth Modeling and Simulation for Switched Circuits*. London, U.K.: Springer-Verlag, 2011.

[15] J. J. Rico-Melgoza, J. P. Suarez, E. Barrera-Cardiel, and M. M. Martinez, "Modeling and analysis of three-phase diode bridge rectifiers as linear complementarity systems," *Electric Power Components and Systems*, vol. 47, no. 15, pp. 1639–1655, 2009.

[16] C. Batlle, E. Fossas, I. Merillas, and A. Miralles, "Generalized discontinuous conduction modes in the complementarity formalism," *IEEE Trans. Circuits Syst. II, Exp. Briefs*, vol. 52, no. 8, pp. 447–451, 2005.

[17] F. López-Castillo and J. J. Rico-Melgoza, "Modeling and analysis of switched networks as mixed linear complementarity systems," in *IEEE Int. Autumn Meeting on Power, Electronics and Computing*, Xtapa, Mexico, Nov 2014, pp. 1–6.

[18] V. Sessa, L. F. C. Monteiro, and D. M. Dias, "A single-phase active filter with cascaded multilevel inverter modelled as a complementarity problem," in *42nd Annual Conf. IEEE Industrial Electronics Soc.*, Florence, Italy, Oct 2016, pp. 1075–1080.

[19] H. S. H. Chung, A. Ioinovici, and J. Zhang, "Describing functions of power electronics circuits using progressive analysis of circuit waveforms," *IEEE Trans. Circuits Syst. I, Reg. Papers*, vol. 47, no. 7, pp. 1026–1037, 2000.